Received: 3 May 2018 | Revised: 24 July 2018 | Accepted: 26 July 2018

DOI: 10.1111/dom.13497

WILEY

ORIGINAL ARTICLE

Cannabinoid-1 receptor regulates mitochondrial dynamics and function in renal proximal tubular cells

Adi Drori | Anna Permyakova | Rivka Hadar | Shiran Udi | Alina Nemirovski | Joseph Tam

Obesity and Metabolism Laboratory, Institute for Drug Research, School of Pharmacy, Faculty of Medicine, The Hebrew University of Jerusalem, Jerusalem, Israel

Correspondence
Joseph Tam, Obesity and Metabolism Laboratory, The Institute for Drug Research, School of Pharmacy, Faculty of Medicine, POB 12065, Jerusalem 9112001, Israel.
Email: yossit@ekmd.huji.ac.il

Funding information
This work was supported by an ERC-2015-StG grant (#676841) as well as a grant from the Israel Science Foundation (ISF; 158/18) to J. T.

Aims: To evaluate the specific role of the endocannabinoid/cannabinoid type-1 (CB_1R) system in modulating mitochondrial dynamics in the metabolically active renal proximal tubular cells (RPTCs).

Materials and methods: We utilized mitochondrially-targeted GFP in live cells (wild-type and null for the CB_1R) and electron microscopy in kidney sections of RPTC-$CB_1R^{-/-}$ mice and their littermate controls. In both in vitro and in vivo conditions, we assessed the ability of CB_1R agonism or fatty acid flux to modulate mitochondrial architecture and function.

Results: Direct stimulation of CB_1R resulted in mitochondrial fragmentation in RPTCs. This process was mediated, at least in part, by modulating the phosphorylation levels of the canonical fission protein dynamin-related protein 1 on both S637 and S616 residues. CB_1R-induced mitochondrial fission was associated with mitochondrial dysfunction, as documented by reduced oxygen consumption and ATP production, increased reactive oxygen species and cellular lactate levels, as well as a decline in mitochondrial biogenesis. Likewise, we documented that exposure of RPTCs to a fatty acid flux induced CB_1R-dependent mitochondrial fission, lipotoxicity and cellular dysfunction.

Conclusions: CB_1R plays a key role in inducing mitochondrial fragmentation in RPTCs, leading to a decline in the organelle's function and contributing to the renal tubular injury associated with lipotoxicity and other metabolic diseases.

KEYWORDS

cannabinoids, cellular research, experimental pharmacology

1 | INTRODUCTION

Mitochondrial morphology is highly dynamic over time, changing rapidly and significantly in response to cellular stress or to altered metabolic demand.[1] Mitochondria are shaped by ongoing fusion and fission events, and the lack of balance between these opposing processes is often detrimental to maintaining mitochondrial homeostasis. In fact, a breach in this balance has been implicated in the onset of many pathological conditions, such as neurodegenerative diseases and aging, as well as obesity and its related kidney injuries (reviewed in References [2] and [3]).

The endocannabinoid (eCB) system plays an important role in energy balance and homeostasis.[4,5] The main eCBs, *N*-arachidonoylethanolamine (AEA) and 2-arachidonoylglycerol (2-AG), evoke many cellular pathways by binding and activating the two G-protein-coupled receptors, cannabinoid type-1 (CB_1R) and type-2 (CB_2R). The eCB/CB_1R system is highly overactive during obesity,[6,7] and both central and peripheral stimulations of this system have been suggested to mediate obesity-related comorbidities, contributing to the development of the metabolic syndrome.[6,8] Recently, we have demonstrated that over-activated CB_1R mediates obesity-induced kidney injury, dysfunction, inflammation and fibrosis by compromising the function of renal proximal tubular cells (RPTCs).[9] RPTCs are metabolically active and reabsorb up to 80% of the solute and water passing through the nephron via specialized ATP-dependent membrane transporters.[10] To meet this high energy demand, RPTCs rely on mitochondrial oxidative phosphorylation (OXPHOS) to produce ATP.[11] Thus, an impairment in mitochondrial bioenergetics may result in renal dysfunction. Indeed, accumulating evidence links mitochondrial

dysfunction to the development and progression of diseases such as acute kidney injury, diabetic nephropathy and chronic kidney disease.[11–17] This is further supported by our recent finding that RPTC dysfunction is accompanied by decreased utilization of fatty acids by mitochondria and impaired ATP production. Notably, these effects are rescued by a peripheral blockade of CB_1R,[9] in agreement with reports by others who describe a role for the eCB/CB_1R system in modulating different aspects of mitochondrial physiology.[18–21] However, direct modulation of mitochondrial dynamics by eCBs has not yet been described. Here, we show that directly stimulating CB_1R modulates mitochondrial dynamics and function in RPTCs. Specifically, activating CB_1R promotes excessive mitochondrial fragmentation by regulating the phosphorylation of dynamin-related protein 1 (DRP1), leading to mitochondrial dysfunction in the kidney. Interestingly, an acute fatty acid overload also induces CB_1R-dependent mitochondrial fragmentation in RPTCs, suggesting a role for the eCB system in mediating the mitochondrial damage associated with renal lipotoxicity.

2 | MATERIALS AND METHODS

2.1 | Animals and experimental protocol

All animal studies were approved by the Institutional Animal Care and Use Committee of the Hebrew University of Jerusalem (AAALAC accreditation #1285). Male, 8–10-week-old RPTC-$CB_1R^{-/-}$ mice[9,22] and their wild-type (WT) littermate controls were used for the in vivo experiments. To activate CB_1R, mice received a single intraperitoneal injection of 10 mg/kg AEA or arachidonyl-2′-chloroethylamide (ACEA) (90050 or 91054, respectively; Cayman Chemicals, Ann Arbor, Michigan). To test the effect of fatty acid flux-induced CB_1R activation on the kidney, mice received a standard diet (STD) (14% fat, 24% protein, 62% carbohydrates; NIH-31 rodent diet) or a high-fat diet (HFD) (60% fat, 20% protein and 20% carbohydrates; Research Diet, D12492) for 7 days. Mice were euthanized by a cervical dislocation under anesthesia, and blood and kidneys were harvested for further analyses.

2.2 | Multi-parameter metabolic assessment

Mice were metabolically assessed using the Promethion High-Definition Behavioral Phenotyping System (Sable Instruments, Inc., Las Vegas, Nevada) as described previously.[9]

2.3 | Cell culture

WT or $CB_1R^{-/-}$-HK-2 cells (human immortalized RPTCs) were maintained in a low glucose DMEM (01-050-1A; Biological Industries, Beit Haemek, Israel) supplemented with 5% FCS, 100 mM glutamine, 100 mM Na-pyruvate and Pen/Strep (Thermo Fisher Scientific, UK). Cells were cultured at 37 °C in a humidified atmosphere of 5% CO_2/95% air. To test the effect of CB_1R activation, cells were seeded in 6-well plates (25×10^4 cells/well) for 24 hours. Then, growth medium was replaced with serum-free medium (SFM) for an additional 12 hours. On the morning of the experiment, the medium was replaced with fresh SFM containing either vehicle (EtOH), 5 μM AEA, 5 μM ACEA or 250 nM JZL195 for 6 hours. To mimic fatty conditions, cells were overloaded with a mixture of fatty acids containing 0.1 mM sodium Oleate (O7501; Sigma Aldrich, St. Louis, Missouri) and sodium Palmitate (P9767; Sigma Aldrich) in a ratio of 2:1 (O:P, respectively), dissolved in 11% free-fatty acid BSA solution (A7030; Sigma Aldrich). At indicated time points, cells were harvested for further analyses as described below.

2.4 | Stable transfection of RPTCs for mitochondrial overexpression of GFP

HK-2 cells were transfected with pLYS1-FLAG-MitoGFP-HA (#50057; Addgene, Cambridge, Massachusetts), using Lipofectamin3000 (L3000-001; Invitrogen, Thermo Fisher Scientific) according to the manufacturer's protocol. Transfected cells were selected with puromycin (1 μg/μL; P8833, Sigma Aldrich). Antibiotic-resistant cells were then sorted for high GFP expression using FACSAria II (Becton Dickinson, Franklin Lakes, New Jersey), were plated, and MitoGFP expression was validated using a IX-73 fluorescent microscope (OLYMPUS).

2.5 | Genetic deletion of CB_1R in RPTCs

HK-2-MitoGFP cells were transfected with CRISPR-CAS9 vector containing a sgRNA sequence to target all human isoforms of *CNR1* (GeneCopeia CS-HCP263432-CG01-01-B) using Lipofectamine3000 (L3000-001, Invitrogen), and were selected with hygromycin (200 μM; H3274, Sigma Aldrich). Antibiotic-resistant cells were then seeded in a single-cell density and were allowed to grow. Single-cell clones were analysed by DNA sequencing and mRNA analysis to confirm the deletion of CB_1R (Figure S1).

2.6 | Electron microscopy

Kidney slices (3 mm) were fixed overnight in 2% paraformaldehyde and 2.5% glutaraldeyde in 0.1 M cacodylate buffer (pH 7.4) at room temperature, and then washed four times in cacodylate buffer. Tissue slices were stained with 1% osmium tetroxide, 1.5% potassium ferricyanide in 0.1 M cacodylate buffer for 1 hour, were washed four times in cacodylate buffer and were dehydrated. Following dehydration, slices were infiltrated with increasing concentrations of Agar 100 resin in propylene oxide, consisting of 25%, 50%, 75% and 100% resin, for 16 hours each, and were then embedded in fresh resin and allowed to polymerize at 60 °C for 48 hours. Embedded tissues in blocks were sectioned with a diamond knife on a Leica Reichert Ultracut S microtome, and ultrathin sections (80 nm) were collected onto 200 Mesh, carbon–formvar-coated copper grids. The sections on grids were sequentially stained with uranyl acetate and lead citrate for 10 minutes each and were viewed with Tecnai 12 TEM 100 kV (Phillips, Eindhoven, The Netherlands) equipped with a MegaView II CCD camera and Analysis version 3.0 software (SoftImaging System GmbH, Münstar, Germany).

2.7 | Extracellular flux analysis

The cellular oxygen consumption rate (OCR) was measured using a Seahorse XF24 Extracellular Flux Analyzer (Seahorse Bioscience, Agilent Technologies, Billerica, Massachusetts). Briefly, WT-MitoGFP and

$CB_1R^{-/-}$-MitoGFP HK-2 cells were seeded in an XF24 cell culture plate (25×10^3 cells/well) and were incubated overnight in a 37 °C humidified incubator with 5% CO_2. Then, vehicle, AEA or O:P was added to the cells in fresh SFM for the indicated times. Basal OCR was measured at the end of the incubation period. Data were calculated from five consecutive measurements, post instrument calibration.

2.8 | Total DNA extraction and mtDNA/nDNA measurement

Cells were harvested using trypsin, and DNA was extracted with a DNeasy Blood & Tissue Kit (69056, QIAGEN) according to the manufacturer's protocol. Isolated DNA served as a template for a qPCR reaction using primer sets for β2-microglobulin (β2m) to amplify nuclear DNA (nDNA) and a D-loop region to amplify mitochondrial DNA (mtDNA). Primers are listed in Table S1.

2.9 | Quantification of mitochondrial morphology

Fluorescence images in .vsi format were processed in ImageJ software using the OlympusViewer Plugin, and were then subjected to analysis with the publicly available ImageJ macro for mitochondrial morphology, Mito-Morphology, designed by Ruben K. Dagda.[23] The macro returns the circularity value for each mitochondrion in the cell and the average circularity value of each measured cell. The average value ± SEM was plotted. The number of replicates is indicated in each figure legend. The perimeter of each mitochondria and the total mitochondrial area were also measured using the same macro. Interconnectivity was calculated as AVG area/perimeter ratio.

Electron microscope images in .tiff format were analysed using Adobe Photoshop C3S software. Images were analysed in RGB mode, and the measurement scale was set according to the image scale bar. Each mitochondrion was marked using the magnetic laso tool, and measurements of area and perimeter were recorded. Circularity was calculated by the software as $4*\pi\left(\frac{area}{perimeter}\right)\hat{}2$, and the value of 1 represents a perfect circle. The length of mitochondria was measured by manually drawing a line along the mitochondrial major axis, using a ruler, and recording the value.

2.10 | Endocannabinoid measurements by LC-MS/MS

eCBs were extracted, purified and quantified in kidney and cells, as described previously.[9] LC–MS/MS was analysed on an AB Sciex (Framingham, Massachusetts) Triple Quad 5500 mass spectrometer coupled with a Shimadzu (Kyoto, Japan) UHPLC System. eCBs were detected in a positive ion mode using electron spray ionization (ESI) and the multiple reaction monitoring (MRM) mode of acquisition.

The levels of each compound were analysed by monitoring multiple reactions. The molecular ion and fragment for each compound were measured as follows: m/z 348.3→62.1 (quantifier) and 91.1 (qualifier) for AEA, m/z 379.3→287.3 (quantifier) and 91.1 (qualifier) for 2-AG, m/z 305.2→91.1 (quantifier) and 77.1 (qualifier) for AA, and m/z 352.3→66.1 (quantifier) and 91.1 (qualifier) for [$^2H_4$] AEA. The levels of AEA, 2-AG and AA in the kidney and cells were measured against standard curves.

2.11 | Statistical analysis

Data are presented as mean ± SEM. Unpaired two-tailed Student's *t*-test was used to determine variations between groups (GraphPad Prism v6 for Windows). Statistical significance was set at $P < 0.05$. Complete Materials and Methods may be found in the Supporting information section at the end of the article.

3 | RESULTS

3.1 | Direct activation of CB_1R impairs mitochondrial architecture of RPTCs

To evaluate the direct role of CB_1R in regulating mitochondrial dynamics in RPTCs, we tested the acute effect of AEA (10 mg/kg, ip) or vehicle in RPTC-$CB_1R^{-/-}$ mice (lacking CB_1R only in the RPTCs)[9] and in their WT littermate controls. Electron micrographs of kidney sections demonstrated extensive alterations in mitochondrial architecture, mainly in mitochondrial fragmentation, following AEA administration (Figure 1A). Whereas WT mice treated with vehicle showed many elongated mitochondria, the mice treated with AEA contained round and shorter mitochondria (quantified in Figure 1B,C). The AEA-induced impairment of mitochondrial morphology was CB_1R dependent, as RPTC-$CB_1R^{-/-}$ mice were protected from these morphological alterations (Figure 1A–C). As AEA is known to be rapidly degraded in vivo, leading to the production of arachidonic acid (AA), which, in turn, may cause mitochondrial fission on its own,[24] we assessed the eCB "tone" in kidneys collected from mice 6 hours following an intraperitoneal injection of AEA. Renal AEA levels remained significantly high in comparison with Veh-treated controls, whereas no changes in the 2-AG and AA levels were found, highlighting the specificity of the effect documented by AEA (Figure S2). Moreover, we repeated the above-mentioned experiment with the highly selective and stable CB_1R agonist, ACEA, and found extensive mitochondrial fragmentation following its administration in vivo (10 mg/kg, ip) (Figure S3), thus supporting the notion that the effect is CB_1R mediated. As AEA was given systemically, we assumed that the CB_1R-induced changes in mitochondrial architecture were not only restricted to the kidney, but could greatly affect the structure and activity of mitochondria elsewhere; indeed, an indirect assessment of mitochondrial activity in vivo revealed that acute AEA treatment resulted in decreased total oxygen consumption only in the WT animals (Figure 1D).

To further investigate the physiological role of the eCB/CB_1R system in mitochondria of RPTCs, we established a cellular model in which CB_1R was deleted from HK-2 cells, stably expressing mitochondrially targeted GFP, using the CRISPR-CAS genome editing technique (Figure S1). In accordance with our in vivo findings, we found striking differences in mitochondrial morphology associated with the presence or absence of and/or with stimulation of CB_1R in vitro. AEA treatment resulted in excessive mitochondrial fragmentation in RPTCs (Figure 1E), indicated by increased mitochondrial circularity, and decreased perimeter and interconnectivity (Figure 1F–H). Interestingly, $CB_1R^{-/-}$-HK-2 cells displayed reduced basal circularity, increased perimeter and a hyper-fused mitochondrial network compared to the WT cells, and AEA failed to induce mitochondrial fragmentation in the null cells. Similar findings were documented in cells treated with ACEA (5 μM), as well as with

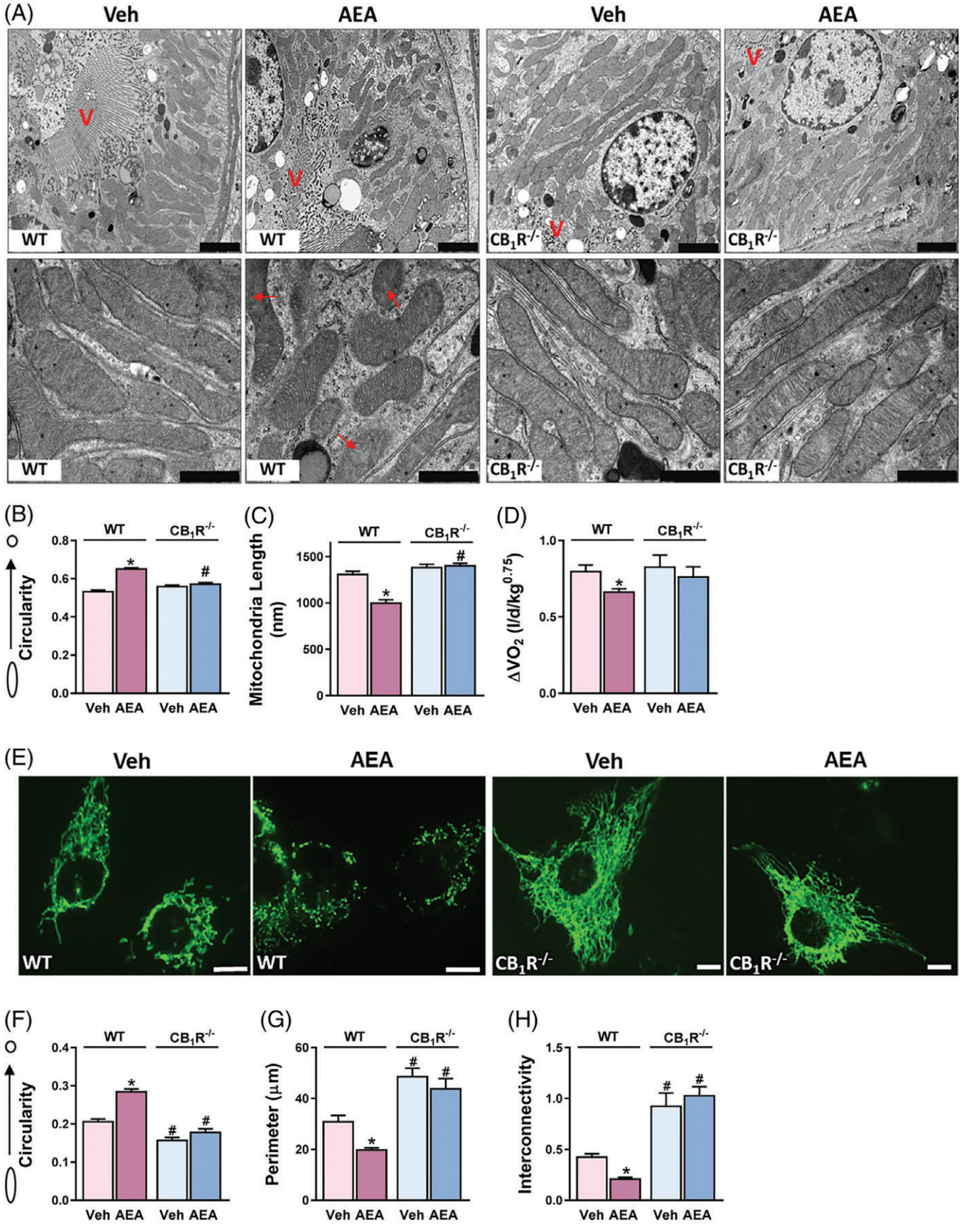

FIGURE 1 Legend on next page.

JZL195, a potent inhibitor of both fatty acid amide hydrolase (FAAH) and monoacylglycerol lipase (MAGL), the primary enzymes responsible for degrading AEA and 2-AG, respectively (Figure S4), suggesting that mitochondrial dynamics in RPTCs are regulated by CB_1R.

3.2 | Acute activation of CB_1R in RPTCs impairs mitochondrial function and biogenesis

As mitochondrial shape is closely related to function, we next evaluated the functional consequence of CB_1R activation on the mitochondria. In vitro AEA treatment resulted in a significant reduction in the basal OCR, and substantially decreased ATP levels in WT-HK-2 cells (Figure 2A,B). Similarly, AEA induced reduction in the NAD^+/NADH ratio (Figure 2C), as well as a 15% increase in cellular lactate content (Figure 2D). All of the mitochondrial malfunctions induced by AEA were absent in $CB_1R^{-/-}$-HK-2 cells. Next, we assessed the effect of AEA on mitochondrial biogenesis, and found that acute activation of CB_1R in WT-HK-2, but not in $CB_1R^{-/-}$-HK-2, cells resulted in a mild, yet significant, reduction in the mtDNA-to-nDNA ratio (Figure 2E). Likewise, the protein expression of two representative mitochondrial respiratory chain components, mtDNA-encoded cytochrome C oxidase I (MTCO1) and nDNA-encoded succinate dehydrogenase complex subunit A (SDHA) was downregulated following AEA exposure in WT-HK-2 cells (Figure 2F). As AEA has been shown to inhibit the proliferation of different cell lines,[25,26] and to induce apoptosis in others,[27,28] we wanted to exclude the possibility that the observed mitochondrial changes resulted from the deleterious effects of AEA on cell viability. Therefore, we performed CFSE staining, followed by FACS analysis, and revealed that AEA did not affect cell proliferation (Figure 2G). Moreover, no increase in the number of early or late apoptotic cells following AEA treatment was documented (Figure 2H). Taken together, our findings suggest that CB_1R-mediated mitochondrial fragmentation is followed by impaired mitochondrial function and reduced biogenesis, without compromising cell viability in the observed time frame.

3.3 | RPTC-CB_1R induces DRP1-mediated mitochondrial fission

To decipher the underlying molecular mechanism involved in CB_1R-induced mitochondrial fragmentation, we assessed the contribution of DRP1, a fundamental component of the fission machinery, to this phenomenon. At the mRNA level, *DRP1* was slightly upregulated by AEA in WT-HK-2 cells (Figure 3A). On the other hand, a reduction in its phosphorylation on S637 was induced by AEA treatment in WT- but not in $CB_1R^{-/-}$-HK-2 cells (Figure 3B,C). Interestingly, the basal ratio between the S637-phosphorylated and total DRP1 in $CB_1R^{-/-}$-HK-2 cells was higher than in the WT-HK-2 cells (Figure 3B,C), concurrent with their hyper-fused mitochondrial network (Figure 1E–H). ACEA and JZL195 also reduced this ratio in a way similar to AEA (Figure S4D,E). When phosphorylated on S637, DRP1 is retained in the cytoplasm and, upon de-phosphorylation, it is translocated to the mitochondria and induces fission.[29,30] Indeed, in a cellular fractionation analysis, AEA treatment led to decreased recovery of both S637-phosphorylated DRP1 and total DRP1 from the cytoplasm of RPTCs, and increased the recovery of total DRP1 from the mitochondrial fraction compared with vehicle-treated cells (Figure 3D). The fractionation fidelity and efficiency were controlled using anti-GFP, which could be recovered only from the mitochondria. Furthermore, by using immune-fluorescence, we found that DRP1 was distributed throughout the cytoplasm in vehicle-treated RPTCs, whereas, in cells treated with AEA, the signal co-localized with HSP60 at the peri-nuclear region, indicating increased mitochondrial localization (Figure 3E,F). No significant changes in the DRP1 expression pattern or cellular localization were documented in $CB_1R^{-/-}$-HK-2 cells treated with AEA.

The inhibitory phosphorylation of DRP1 on S637 is dependent on protein kinase A (PKA),[30,31] whose activity is decreased when CB_1R is stimulated,[32,33] providing a possible explanation for the involvement of CB_1R in this process. Moreover, activating CB_1R and inhibiting PKA, in turn, may lead to increased phosphorylation and the subsequent activity of $ERK_{1/2}$, which was recently shown to directly phosphorylate DRP1 on S616 to promote fission.[34,35] Indeed, AEA treatment increased the phosphorylated-to-total $ERK_{1/2}$ ratio (Figure 3G,H) as well as the levels of S616-phosphorylated DRP1 (Figure 3I,J) in WT-HK-2 cells, but not in $CB_1R^{-/-}$-HK-2 cells, indicating that this signaling cascade is also involved in DRP1-induced mitochondrial fragmentation in RPTCs. Taken together, our findings suggest that CB_1R plays a pivotal role in inducing mitochondrial fission, via regulation of DRP1 phosphorylation or dephosphorylation and its cellular localization.

3.4 | CB_1R-mediated mitochondrial fragmentation is cAMP-dependent

To further corroborate the PKA signaling pathway in this process, we treated both cell lines with Forskolin, a potent inducer of cAMP generation. As expected, this treatment resulted in reduced mitochondrial circularity in both WT-HK-2 and $CB_1R^{-/-}$-HK-2 cells (Figure 4A,B), an

FIGURE 1 | Direct activation of CB_1R impairs mitochondrial architecture of RPTCs. Male, RPTC-$CB_1R^{-/-}$ mice and their WT littermate controls received an intraperitoneal injection of either vehicle (Veh) or 10 mg/kg AEA. A, Mice were euthanized 6 hours after drug administration and their kidneys were processed for electron microscopy. Note: A disrupted mitochondrial morphology was induced by AEA treatment in WT mice only. Scale bar, 2 μm (in upper x3.9 k images) and 1 μm (in lower x23k images). Legend: V, brush border villi; red arrows, obstructed cristae. B,C, mitochondrial circularity and length were measured with adobe Photoshop C3S software. Data represent mean ± SEM of 400–700 mitochondria from 8–10 RPTCs from 2–3 mice per treated group. D, Mice were monitored by the Promethion High-Definition Behavioral Phenotyping System (Sable Instruments, Inc.) over 6 hours. VO_2, normalized to an effective body mass, was calculated. Data represent the mean ± SEM from 7–9 animals per group. E, WT-HK-2 or $CB_1R^{-/-}$-HK-2 cells were stably transfected with MitoGFP and treated with either Veh or 5 μM AEA for 6 hours. Live cells were examined under a fluorescent microscope to visualize mitochondrial morphology. F–H, mitochondrial circularity, perimeter and interconnectivity were measured using a publicly available ImageJ macro for mitochondrial morphology.[23] Data represent the mean ± SEM from 30–65 cells in each group. Scale bar, 10 μm. $^*P < 0.05$ relative to Veh-treated animals or HK-2 of the same cell line. $^{\#}P < 0.05$ relative to the same treated group in WT mice or HK-2 cells

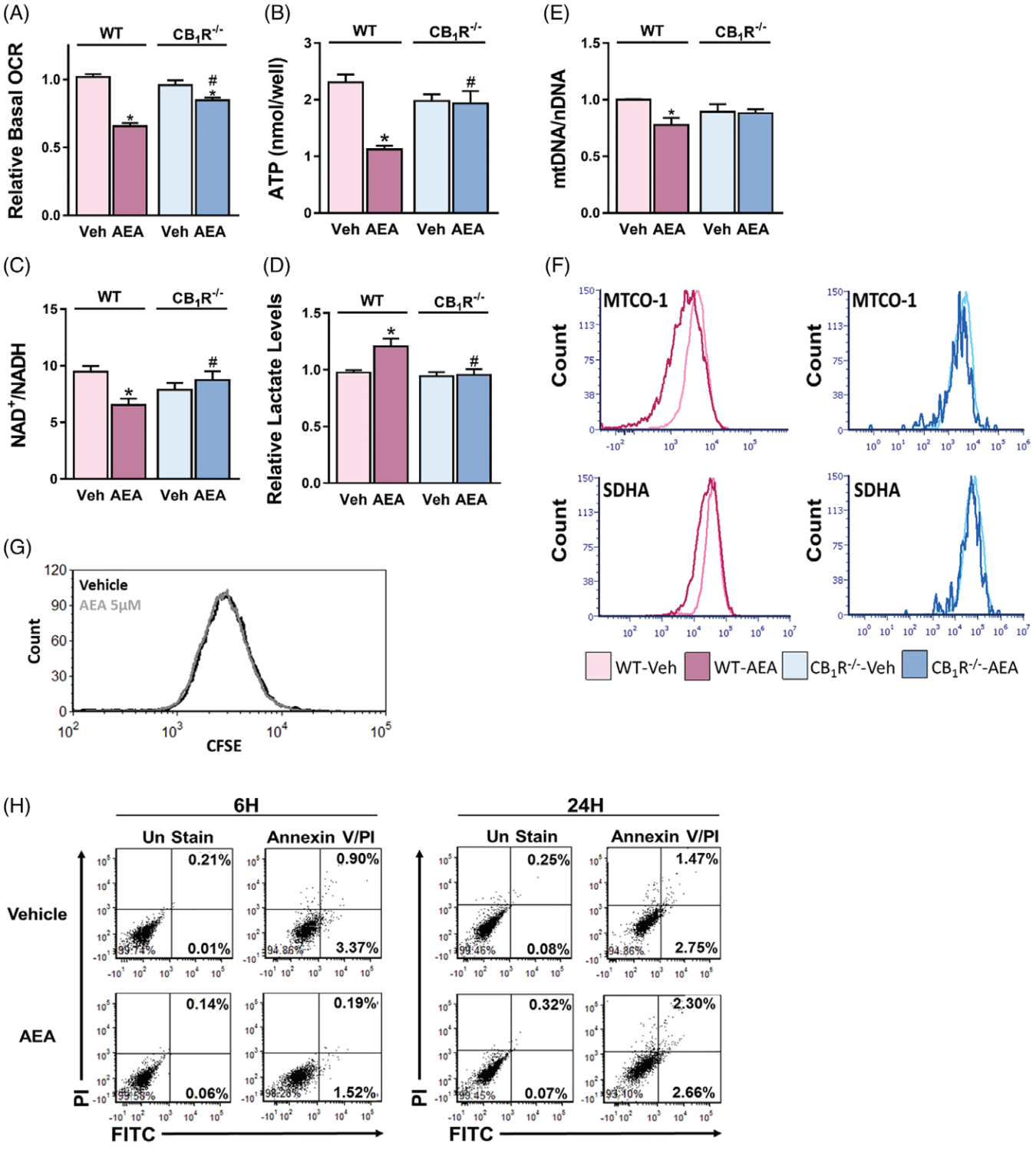

FIGURE 2 Acute activation of CB_1R in HK-2 cells impairs mitochondrial function and biogenesis. WT-HK-2 or $CB_1R^{-/-}$-HK-2 cells were treated with either vehicle (Veh) or 5 μM AEA for 6 hours and were then analysed for mitochondrial function. A, Reduced oxygen consumption rate (OCR) measured using the Seahorse XF analyzer, B, reduced ATP levels, and C, reduced NAD^+/NADH ratio, as well as D, elevated cellular lactate levels, were found in WT-HK-2 cells treated with AEA (5 μM). Data represent the mean ± SEM of at least six replicates from three independent experiments. E, The ratio between mitochondrial and nuclear DNA. F, FACS analysis for MTCO-1 and SDHA, demonstrating reduced biogenesis following treatment of wild-type cells with AEA. G, H, WT-HK-2 cells, exposed to Veh or 5 μM AEA, were analysed by flow cytometry for proliferation (G) with CFSE staining after 24 hours of treatment or for apoptosis (H) with Annexin V and Propidium Iodide at the indicated time points. Data represent one experiment out of three performed (in triplicate). $^*P < 0.05$ relative to Veh-treated HK-2 of the same cell line. $^{\#}P < 0.05$ relative to the same treated group in WT-HK-2 cells

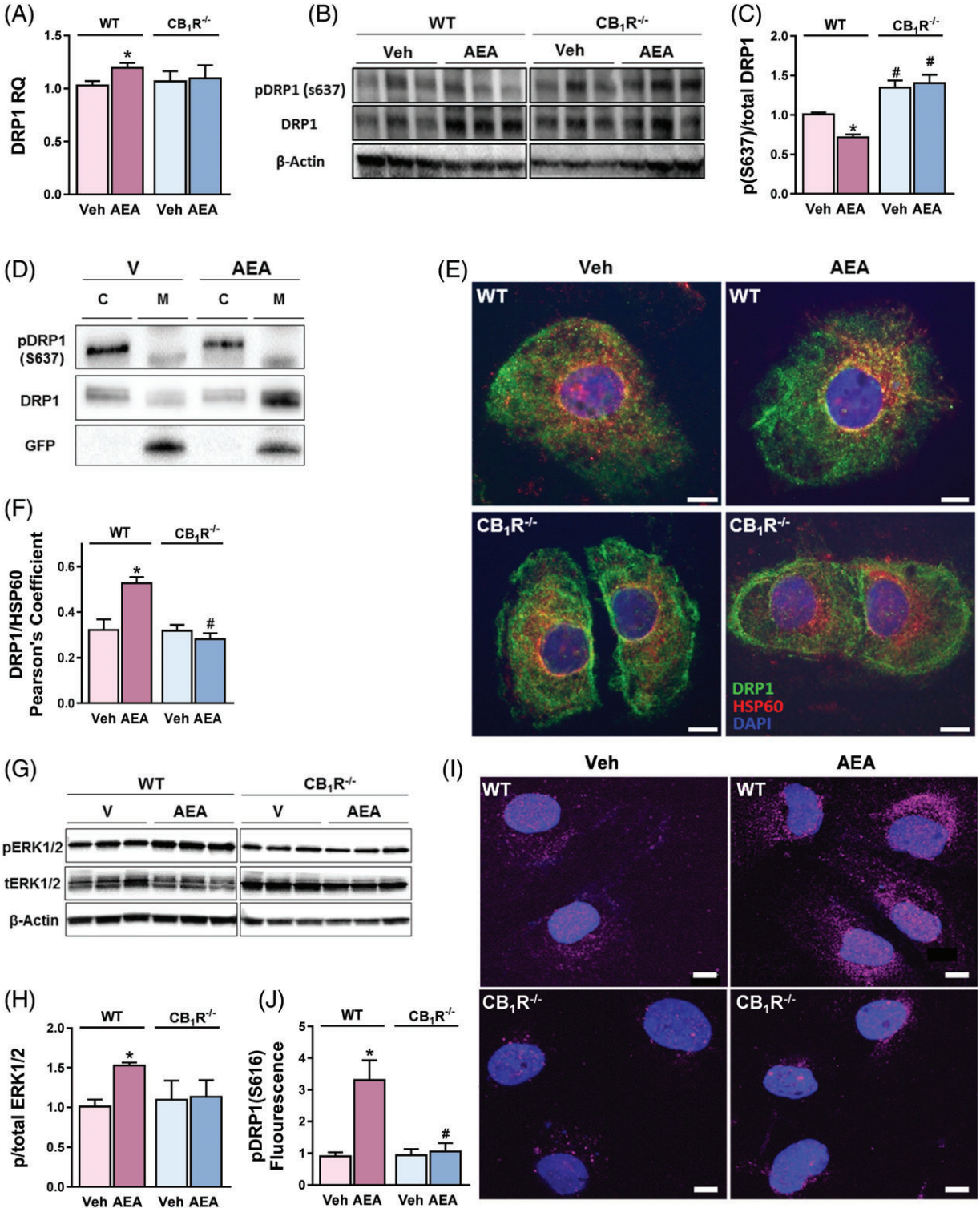

FIGURE 3 RPTC-CB_1R induces DRP1-mediated mitochondrial fission. A, qPCR analysis of *DRP1*. B,C, Reduced expression of the phosphorylated (S637) form of DRP1 was measured in AEA (5 μM)-treated WT-HK-2 cells. D, Cellular fractionation revealed increased localization of DRP1 in the mitochondria of RPTCs treated with AEA. E, Co-staining of HSP60 and DRP1 in RPTCs. F, Co-localization was quantified by calculating Pearson correlation coefficient [P(r)] of two fluorescent signals using CellSens Dimension Software. G,H, Increased phosphorylation of $ERK_{1/2}$, as well as I, J, DRP1 (S616), in RPTCs treated with AEA. Data represent the mean ± SEM of at least five replicates from two–three independent experiments. $^{*}P < 0.05$ relative to Veh-treated animals or HK-2 of the same cell line. $^{\#}P < 0.05$ relative to the same treated group in WT mice or HK-2 cells. B, G Representative images from three–five independent experiments performed in triplicates

effect that could be attributed to increased S637 phosphorylation of DRP1 (Figure 4C,D). The decreased circularity was reversed by AEA treatment in WT-HK-2 cells only, but not in HK-2 cells lacking the CB_1R (Figure 4A,B). Moreover, direct inhibition of PKA with H-89 induced mitochondrial fragmentation (Figure 4E,F) and reduced S637 phosphorylation (Figure 4G,H) in both cell lines, suggesting that PKA is located downstream of CB_1R and upstream of DRP1 in this cascade.

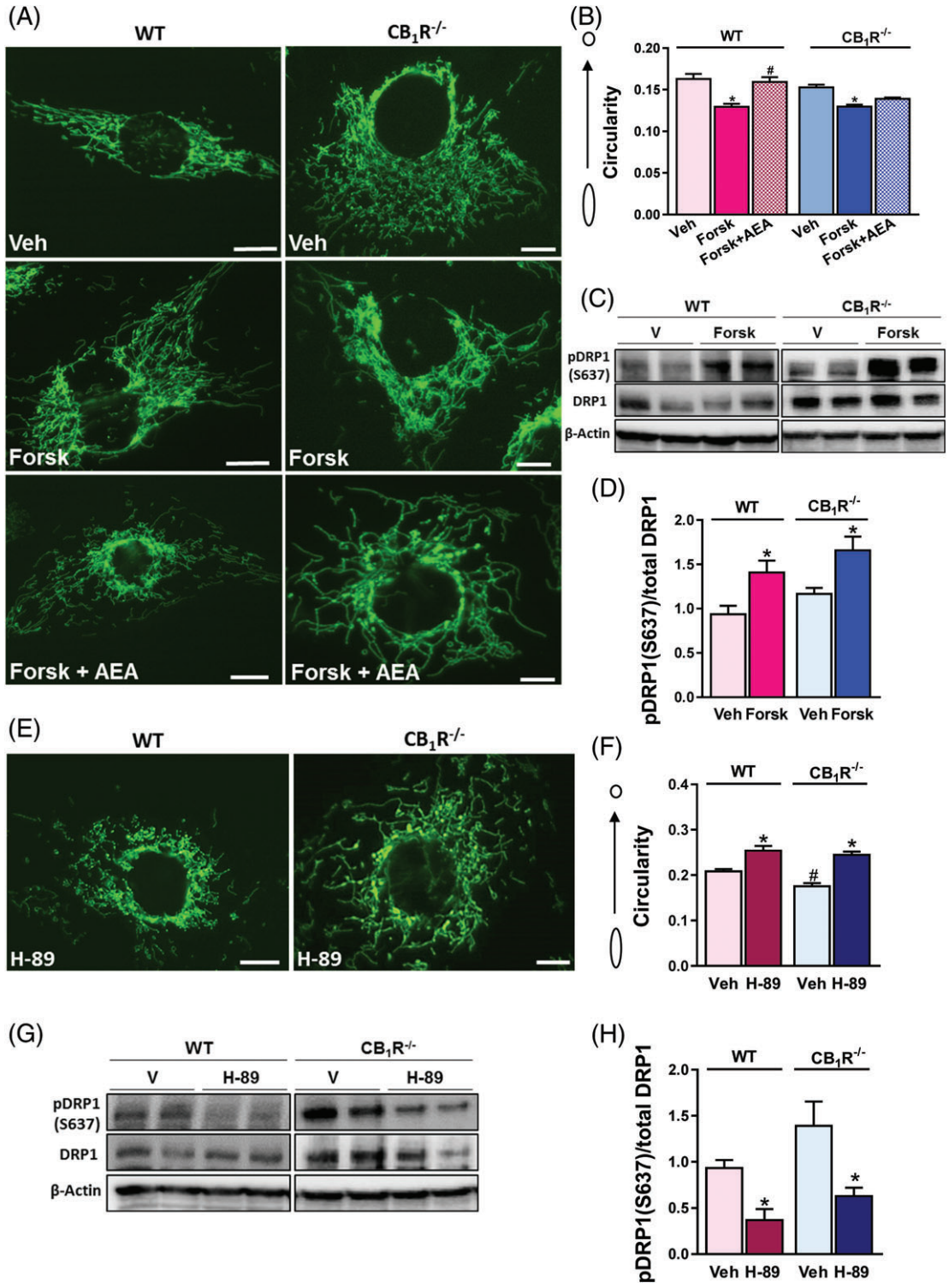

FIGURE 4 CB_1R-mediated mitochondrial fragmentation is cAMP-dependent. A, WT-HK-2 or $CB_1R^{-/-}$-HK-2 cells, stably transfected with MitoGFP, were treated with vehicle (Veh) or 25 μM Forskolin for 1 hour to induce cAMP generation. AEA was then added to selected wells and live cells were examined under a fluorescent microscope to visualize mitochondrial morphology. B, Circularity was quantified using ImageJ macro.[23] Data represent the mean ± SEM from >30 cells in each group. C, D, Western blot analysis and quantification of pDRP1 (s637). E, 10 μM of H-89 were added to both cell lines for 3 hours, and F, circularity was quantified using ImageJ macro.[23] Data represent the mean ± SEM from 30–120 cells in each group. G, H, Western blot analysis and quantification of pDRP1 (s637). Western blot data represent the mean ± SEM of four–five replicates from two independent experiments. $^{*}P < 0.05$ relative to Veh-treated animals or HK-2 of the same cell line. $^{\#}P < 0.05$ relative to the same treated group in WT mice or HK-2 cells

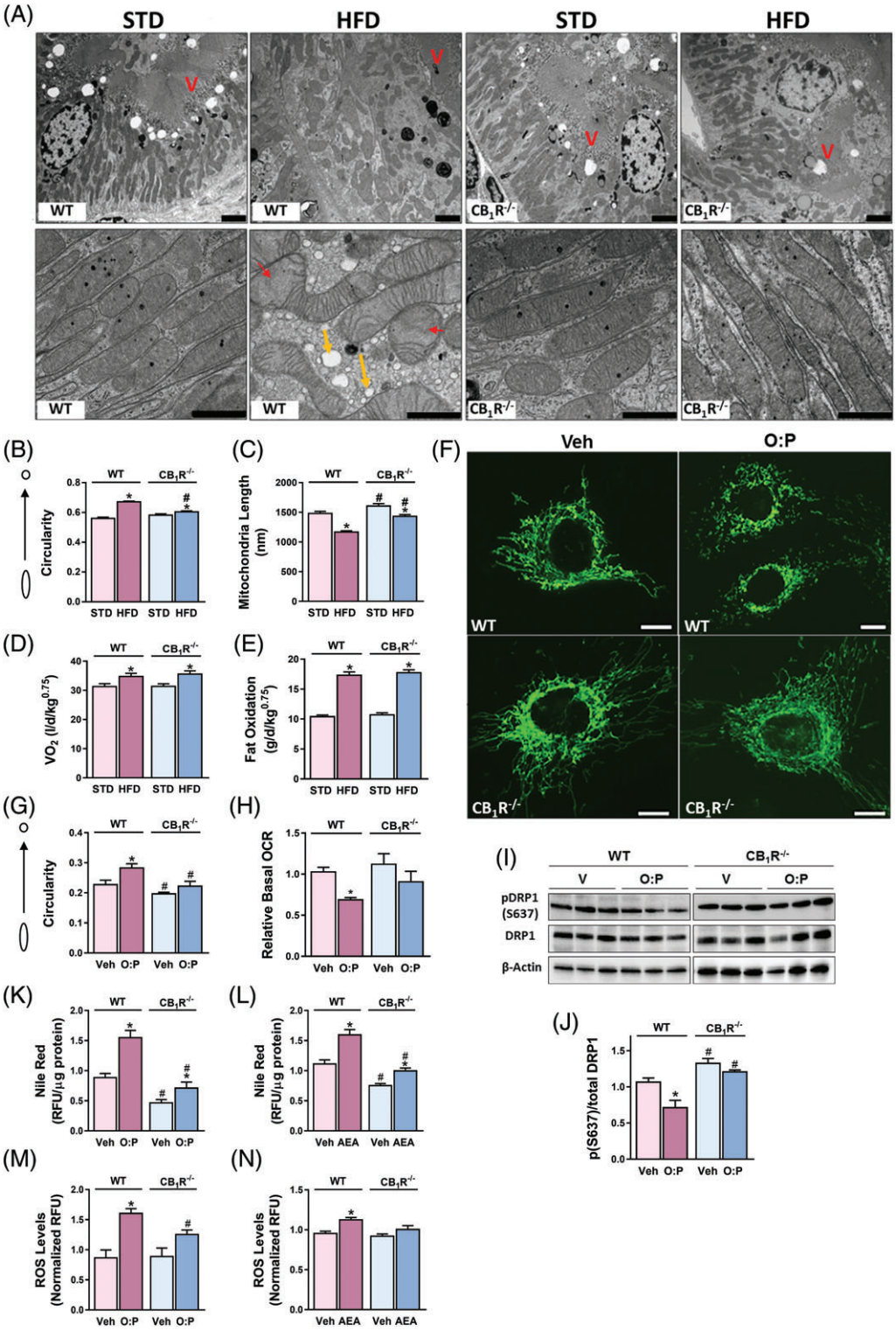

FIGURE 5 Legend on next page.

3.5 | Deletion of CB_1R ameliorates fatty acid-induced mitochondrial fragmentation in RPTCs

High-fat diet (HFD) feeding was shown to induce vast changes in mitochondrial architecture in the kidney, leading to proximal tubular injury and glomerulopathy.[36] We recently reported that CB_1R blockade protects against HFD-induced reduction in mitochondrial fatty acid β-oxidation and ATP production.[9] This, together with the current data, encouraged us to explore the possibility that the eCB/CB_1R system is also involved in HFD-mediated changes in mitochondrial architecture. Specifically, we evaluated the effect of an acute fatty acid overload on mitochondrial dynamics in RPTCs both in vivo and in vitro. To that end, we fed RPTC-$CB_1R^{-/-}$ mice and their WT littermate controls with either STD or HFD for a short-term period, and followed mitochondrial shape and fat accumulation in the RPTCs. Interestingly, HFD-fed WT animals exhibited an extensive impairment

of mitochondrial morphology in RPTCs, while RPTC-$CB_1R^{-/-}$ mice were almost completely protected from these alterations (Figure 5A). These alterations included increased mitochondrial circularity (Figure 5B) and reduced mitochondrial length (Figure 5C), as well as increased accumulation of fat droplets within RPTCs (Figure 5A, yellow arrows). As expected, both mouse strains gained a similar body weight (data not shown), as well as increased whole-body oxygen consumption and total fat oxidation (Figure 5D,E). Likewise, mitochondrial fragmentation was documented in an in vitro model for fatty acid flux, in which wild-type-MitoGFP or $CB_1R^{-/-}$-MitoGFP HK-2 cells were incubated with a mixture of 0.1 mM O:P for 24 hours. The exposure to O:P resulted in excessive mitochondrial fragmentation (Figure 5F, G), and reduced basal OCR (Figure 5H), conferring the same functional decline as a direct activation of CB_1R (Figure 1D). Additionally, reduced levels of DRP1 S637 phosphorylation in the WT-HK2 cells was documented (Figure 5I,J). Conversely, HK-2 cells that do not express CB_1R had significantly lower circularity scores in response to O:P (Figure 5G), with no significant changes in basal OCR or DRP1-S637 phosphorylated levels, suggesting that CB_1R mediates the changes documented in mitochondrial architecture that were induced by increased fatty acid flux. Interestingly, both direct and fatty acid-induced activation of CB_1R in wild type cells resulted in intracellular lipid accumulation (Figure 5K,L) and elevated levels of reactive oxygen species (Figure 5M,N), which are often associated with mitochondrial dysfunction,[37,38] supporting a common mechanism that mediates mitochondrial damage in both experimental models.

4 | DISSCUSSION

The ability of the eCB/CB_1R system to regulate energy balance and metabolism is well established, including its effects on appetite[39,40] and energy expenditure.[41] These effects are not only limited to central regulation, because the eCB system, specifically via the CB_1R, controls cellular metabolism in peripheral organs also, including the liver, adipose tissue and kidney.[42–46] Whereas several lines of investigation suggest that the eCB/CB_1R system regulates bioenergetics by directly regulating mitochondrial function (reviewed in Reference 19), no evidence implicating mitochondrial dynamics in this phenomenon has yet been reported. Here, we documented, for the first time, the involvement of CB_1R in regulating mitochondrial morphology and assessed its relevance to renal lipotoxicity.

Previous reports clearly link altered metabolic flux with mitochondrial shape and function (reviewed in Reference 47). Specifically, metabolic insults, such as elevated levels of glucose[48,49] or fatty acids,[50] result in mitochondrial fragmentation and dysfunction. As CB_1R activation recapitulates the conditions of excess nutrients, it was very exciting to discover that AEA, its stable analog, ACEA, or increased eCB "tone" induces excessive mitochondrial fragmentation in RPTCs. This notion is further supported by our findings that short-term HFD feeding in vivo and acute exposure to fatty acids in vitro result in mitochondrial fragmentation, mediated also via the CB_1R. Similarly, long-term HFD feeding has been shown to induce mitochondrial fragmentation in the kidney,[36] and treating obese mice with SS-31, which protects cristae structure, preserves mitochondrial architecture and restores normal mitochondrial function,[36] emphasizing the tight link between architecture and function. Likewise, our findings suggest that activating the eCB system via CB_1R may link fatty acid flux with mitochondrial fragmentation. These findings are of great importance, considering the well-documented contribution of mitochondrial dysfunction to the development of kidney injury,[15–17,51,52] making CB_1R a compelling target for treating lipotoxicity-related kidney damage. Indeed, our recent work supports this notion as peripheral CB_1R blockade, as well as its specific genetic deletion from RPTCs, ameliorates obesity-induced kidney dysfunction, inflammation and tubulointerstitial fibrosis by preventing lipid accumulation and subsequent lipotoxicity, which is associated with abnormal mitochondrial function of RPTCs.[9] The current work further highlights the contribution of CB_1R-induced mitochondrial fragmentation to such cellular damage. These findings could generally be associated with regulating energy utilization because the kidneys are second only to the heart in mitochondrial abundance and oxygen consumption,[53] and because the RPTCs constitute approximately half of the kidney mass and use the majority of oxygen consumed by the organ.[54]

A link between mitochondrial morphology and bioenergetics was first reported decades ago,[55] with a substantial amount of supporting data accumulating ever since. The relationship between the two mitochondrial features is reciprocal, as evident from studies showing that manipulation of mitochondrial dynamics led to deficiencies in

FIGURE 5 | Deletion of CB_1R ameliorates fatty acid-induced mitochondrial fragmentation in RPTCs. Male RPTC-$CB_1R^{-/-}$ mice and their WT littermate controls received STD or HFD for 7 days. A, Kidneys were processed for electron microscopy. Disrupted mitochondrial morphology induced by HFD feeding was documented only in WT mice. Scale bar, 2 μm (in upper x3.9 k images) and 1 μm (in lower in x23k images). Legend: V, Brush border villi; red arrows, obstructed cristae; yellow arrows, lipid vacuoles. B,C, Mitochondrial circularity and length were measured with Adobe Photoshop C3S software. Data represent mean ± SEM of at least 300 mitochondria from 5–7 RPTCs per group. D, E, Mice were monitored by the Promethion High-Definition Behavioral Phenotyping System (Sable Instruments, Inc.) over the last 24 hours of the experiment. VO_2 and total fat oxidation, normalized to an effective body mass, were calculated. Data represent the mean ± SEM from four–six animals per group. F, WT-HK-2 or $CB_1R^{-/-}$-HK-2 cells stably transfected with MitoGFP were examined under a fluorescent microscope to visualize mitochondrial morphology following an exposure to 0.1 mM mixture of O:P for 24 hours. Representative images from three independent experiments performed in triplicates. Scale bar, 10 μm. G, Circularity was quantified using ImageJ macro.[23] Data represent the mean ± SEM from >20 cells for each group. H, Reduced oxygen consumption rate (OCR) in WT-HK-2 cells treated with fatty acids, as measured by the Seahorse XF analyzer. I, J, Reduced expression of the phosphorylated (S637) form of DRP1 was measured in O:P-treated WT-HK-2 cells. K, L Quantification of intracellular fat accumulation following O:P and AEA treatment by using Nile-Red staining. M, N, ROS production was measured in cell lysates using commercial kits, as described in the methods section (Supporting Information). Data represents mean ± SEM of at least 15 replicates per group, from three independent experiments. $^{*}P < 0.05$ relative to Veh-treated animals or HK-2 of the same cell line. $^{\#}P < 0.05$ relative to the same treated group in WT mice or HK-2 cells

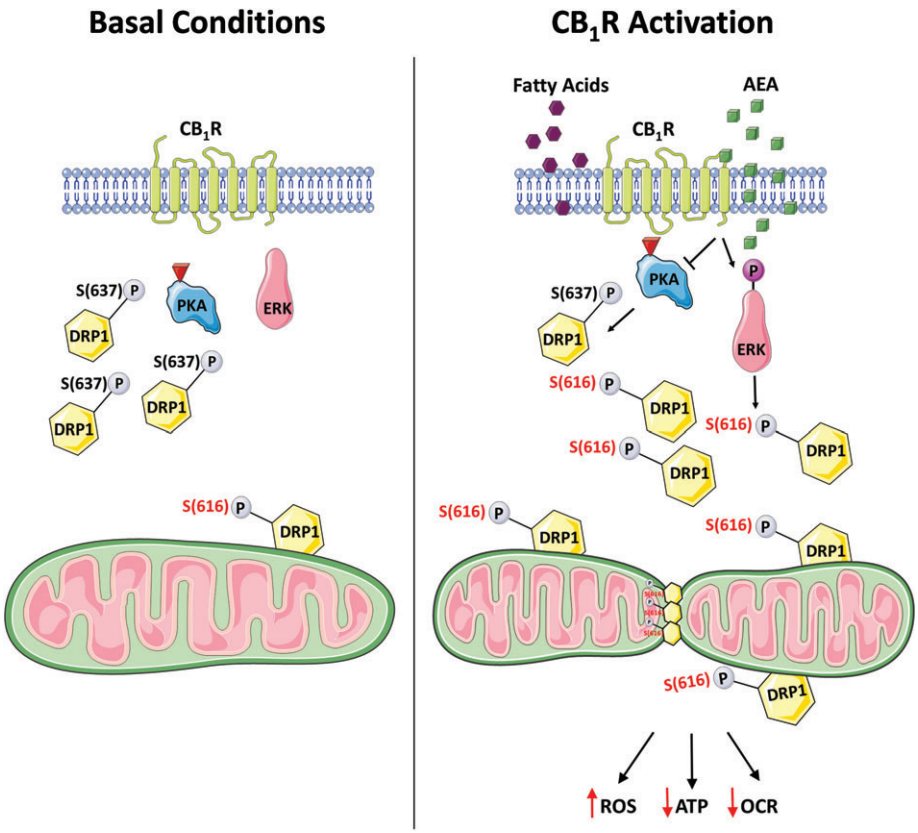

FIGURE 6 Suggested mechanism linking CB_1R and mitochondrial dynamics. Left panel describes normal conditions in which PKA is active, thereby phosphorylating DRP1 on S637. This inhibitory phosphorylation retains DRP1 in the cytoplasm and fission is limited. Right panel describes either a direct activation of CB_1R with AEA or a fatty acid flux-induced indirect activation of CB_1R that inhibits PKA, leading to decreased phosphorylation of S637, which allows DRP1 to target mitochondria and induce fission. PKA inhibition subsequently activates $ERK_{1/2}$, which phosphorylates DRP1 on S616, further promoting fission. Excessive mitochondrial fragmentation under these conditions is followed by a functional decline of mitochondria

mitochondrial respiration and ATP depletion.[56] In contrast, a few studies reported that inhibiting complex I, or complementing it genetically, can affect mitochondrial fragmentation.[1,57] In accordance with recent reports demonstrating that AEA induces reduced OXPHOS and ATP production,[58,59] we documented here reduced OCR, as well as reduced ATP levels and the NAD^+/NADH ratio in WT- but not in $CB_1R^{-/-}$-HK-2 cells treated with AEA, suggesting a functional decline in mitochondrial respiration following CB_1R activation.

Previous studies have linked activated CB_1R with decreased mitochondrial biogenesis in other tissues.[21,60] Similarly, we found decreased mtDNA content and mitochondrial protein expression following treatment of WT-HK-2 cells with AEA. However, we could not detect any appreciable changes in the mRNA expression levels of Complex I or Complex IV components (data not shown). Taken together, these findings support the key role of CB_1R in modulating mitochondrial function and, possibly, biogenesis. Notably, we cannot rule out the involvement of enhanced autophagy rather than impaired biogenesis in reducing mitochondrial content.

Our findings are also in agreement with those of others (reviewed in Reference 61) who describe the role of the eCB system in regulating ROS production and the redox state. Whereas several studies reported that activating the eCB system confers protection from oxidative stress,[62,63] others demonstrated that its stimulation results in ROS generation and cell death.[20,28] Interestingly, Mukhopadhyay and colleagues found that pharmacological inhibition or genetic deletion of CB_1R alleviates cisplatin-induced kidney injury by attenuating MAPK activation and, consequently, cell death associated with oxidative stress.[64] As AEA also activates CB_2R and interacts with other membrane receptors, ion channels and effector proteins,[65] it is possible that some of the AEA-induced changes are mediated via other receptors. In fact, there is evidence that AEA also exerts some of its actions in CB_1R null mice.[65] Nevertheless, as most of the effects of AEA observed here were negated in RPTC-$CB_1R^{-/-}$ mice and in $CB_1R^{-/-}$-HK-2 cells, as well as the fact that both ACEA- and JZL195-induced eCB production resulted in a similar degree of mitochondrial fragmentation in RPTCs, off-target effects are less likely to mediate the entire phenomenon described here.

The observed CB_1R-dependent mitochondrial fragmentation is mediated, at least in part, by regulating the phosphorylation levels of DRP1, one of the key post-translational modifications of DRP1. Our findings are in agreement with studies showing that PKA-mediated phosphorylation of S637 inhibits fission by retaining DRP1 in the cytoplasm.[30,31] On the other hand, others have demonstrated that phosphorylation of the same conserved residue by CaMKIIα or ROCK1 enhances DRP1 recruitment to mitochondria,[66,67] therefore promoting fission. This alleged contradiction most likely suggests that the functional consequence of DRP1 phosphorylation on its activity is stimulus and/or cell-type dependent. The peri-nuclear accumulation

of both S616-phosphorylated and total-DRP1 following CB_1R stimulation further supports enhanced fission, as such peri-nuclear clustering of fragmented mitochondria following the induction of fission has been reported previously.[68]

After CB_1R was identified as a classic plasma membrane receptor, the effects of cannabinoids on mitochondrial function were thought to be either the indirect result of stimulating CB_1Rs present on the plasma membrane or the result of unspecific changes in the mitochondrial membranes by these lipid ligands.[69] Conversely, consistent evidence shows that mitochondria contain G proteins and their downstream effectors. In fact, 30% of neuronal mitochondria carry CB_1Rs ($mtCB_1R$), and both Δ^9-THC and eCBs suppress electron transport complex I activity and respiration in isolated mitochondria, probably by reducing cAMP levels and PKA activity.[70] Since this initial discovery, others have suggested the presence of CB_1Rs in the mitochondria of different organs.[71,72] Whether cannabinoids also modulate mitochondrial dynamics via a direct effect on $mtCB_1R$ in RPTCs remains to be determined, and we are currently conducting studies to elucidate this phenomenon.

In conclusion, our data describe a novel role for CB_1R in modulating mitochondrial physiology by regulating the phosphorylation levels of DRP1 (Figure 6). We suggest that a direct CB_1R activation, or a fatty environment, indirectly, may inhibit the activity of PKA, thereby reducing the phosphorylation of DRP1 on S637. In addition, CB_1R stimulation led to increased phosphorylation of $ERK_{1/2}$ which, in turn, may contribute to the enhanced phosphorylation of DRP1 on S616. Consequently, increased mitochondrial fission occurs, leading to deterioration in mitochondrial function. This, in turn, may lead to RPTC dysfunction, documented in obesity and other metabolic diseases associated with kidney damage.

ACKNOWLEDGMENTS

We are grateful to Dr Yael Friedman from the Bio-Imaging Unit, The Alexander Silberman Institute of Life Science of the Hebrew University for her technical assistance with transmission electron microscopy. We also appreciate the insights and assistance of Mr Dekel Assaf in implementing the quantification methods of mitochondrial morphology described in this work as well as the technical assistance of Dr Liad Hinden and Mr Shahar Azar.

Conflict of interest

The authors declare that no conflict of interest exists.

Author contributions

A. D. conducted the experiments and analysed the data. A. P. assisted in conducting the experiments. S. U. conducted and analyzed the in vivo metabolic assessment. R. H. provided reagents and technical assistance. A. N. conducted the LC–MS/MS analysis. A. D. and J. T. designed and supervised the experiments and wrote the manuscript.

ORCID

Joseph Tam http://orcid.org/0000-0002-0948-0093

REFERENCES

1. Benard G, Bellance N, James D, et al. Mitochondrial bioenergetics and structural network organization. *J Cell Sci*. 2007;120:838-848.
2. Wai T, Langer T. Mitochondrial dynamics and metabolic regulation. *Trends Endocrinol Metab*. 2016;27:105-117.
3. Liesa M, Shirihai OS. Mitochondrial dynamics in the regulation of nutrient utilization and energy expenditure. *Cell Metab*. 2013;17:491-506.
4. Fride E, Bregman T, Kirkham TC. Endocannabinoids and food intake: newborn suckling and appetite regulation in adulthood. *Exp Biol Med*. 2005;230:225-234.
5. Pagotto U, Marsicano G, Cota D, Lutz B, Pasquali R. The emerging role of the endocannabinoid system in endocrine regulation and energy balance. *Endocr Rev*. 2006;27:73-100.
6. Engeli S, Bohnke J, Feldpausch M, et al. Activation of the peripheral endocannabinoid system in human obesity. *Diabetes*. 2005;54:2838-2843.
7. Engeli S. Dysregulation of the endocannabinoid system in obesity. *Neuroendocrinology*. 2008;20(suppl 1):110-115.
8. Pagotto U, Vicennati V, Pasquali R. The endocannabinoid system and the treatment of obesity. *Ann Med*. 2005;37:270-275.
9. Udi S, Hinden L, Earley B, et al. Proximal tubular cannabinoid-1 receptor regulates obesity-induced CKD. *J Am Soc Nephrol*. 2017;28:3518-3532.
10. Weiland C, Ahr HJ, Vohr HW, Ellinger-Ziegelbauer H. Characterization of primary rat proximal tubular cells by gene expression analysis. *Toxicol In Vitro*. 2007;21:466-491.
11. Higgins GC, Coughlan MT. Mitochondrial dysfunction and mitophagy: the beginning and end to diabetic nephropathy? *Br J Pharmacol*. 2014;171:1917-1942.
12. Casemayou A, Fournel A, Bagattin A, et al. Hepatocyte nuclear factor-1beta controls mitochondrial respiration in renal tubular cells. *J Am Soc Nephrol*. 2017;28:3205-3217.
13. Bonventre JV, Yang L. Cellular pathophysiology of ischemic acute kidney injury. *J Clin Invest*. 2011;121:4210-4221.
14. Kanwar YS, Sun L, Xie P, Liu FY, Chen S. A glimpse of various pathogenetic mechanisms of diabetic nephropathy. *Annu Rev Pathol*. 2011;6:395-423.
15. Weinberg JM. Mitochondrial biogenesis in kidney disease. *J Am Soc Nephrol*. 2011;22:431-436.
16. Zhan M, Brooks C, Liu F, Sun L, Dong Z. Mitochondrial dynamics: regulatory mechanisms and emerging role in renal pathophysiology. *Kidney Int*. 2013;83:568-581.
17. Hall AM, Unwin RJ. The not so 'mighty chondrion': emergence of renal diseases due to mitochondrial dysfunction. *Nephron Physiol*. 2007;105:1-10.
18. Hebert-Chatelain E, Desprez T, Serrat R, et al. A cannabinoid link between mitochondria and memory. *Nature*. 2016;539:555-559.
19. Lipina C, Irving AJ, Hundal HS. Mitochondria: a possible nexus for the regulation of energy homeostasis by the endocannabinoid system? *Am J Physiol Endocrinol Metab*. 2014;307:E1-E13.
20. Siegmund SV, Qian T, de Minicis S, et al. The endocannabinoid 2-arachidonoyl glycerol induces death of hepatic stellate cells via mitochondrial reactive oxygen species. *FASEB J*. 2007;21:2798-2806.
21. Tedesco L, Valerio A, Dossena M, et al. Cannabinoid receptor stimulation impairs mitochondrial biogenesis in mouse white adipose tissue, muscle, and liver: the role of eNOS, p38 MAPK, and AMPK pathways. *Diabetes*. 2010;59:2826-2836.
22. Hinden L, Udi S, Drori A, et al. Modulation of renal GLUT2 by the cannabinoid-1 receptor: implications for the treatment of diabetic nephropathy. *J Am Soc Nephrol*. 2018;29:434-448.
23. Dagda RK, Cherra SJ III, Kulich SM, Tandon A, Park D, Chu CT. Loss of PINK1 function promotes mitophagy through effects on oxidative stress and mitochondrial fission. *J Biol Chem*. 2009;284:13843-13855.
24. Cereghetti GM, Costa V, Scorrano L. Inhibition of Drp1-dependent mitochondrial fragmentation and apoptosis by a polypeptide antagonist of calcineurin. *Cell Death Differ*. 2010;17:1785-1794.
25. Laezza C, Pisanti S, Crescenzi E, Bifulco M. Anandamide inhibits Cdk2 and activates Chk1 leading to cell cycle arrest in human breast cancer cells. *FEBS Lett*. 2006;580:6076-6082.

26. Ligresti A, Bisogno T, Matias I, et al. Possible endocannabinoid control of colorectal cancer growth. *Gastroenterology*. 2003;125:677-687.
27. Patsos HA, Greenhough A, Hicks DJ, et al. The endogenous cannabinoid, anandamide, induces COX-2-dependent cell death in apoptosis-resistant colon cancer cells. *Int J Oncol*. 2010;37:187-193.
28. Rajesh M, Mukhopadhyay P, Hasko G, Liaudet L, Mackie K, Pacher P. Cannabinoid-1 receptor activation induces reactive oxygen species-dependent and -independent mitogen-activated protein kinase activation and cell death in human coronary artery endothelial cells. *Br J Pharmacol*. 2010;160:688-700.
29. Chang CR, Blackstone C. Dynamic regulation of mitochondrial fission through modification of the dynamin-related protein Drp1. *Ann N Y Acad Sci*. 2010;1201:34-39.
30. Cribbs JT, Strack S. Reversible phosphorylation of Drp1 by cyclic AMP-dependent protein kinase and calcineurin regulates mitochondrial fission and cell death. *EMBO Rep*. 2007;8:939-944.
31. Chang CR, Blackstone C. Cyclic AMP-dependent protein kinase phosphorylation of Drp1 regulates its GTPase activity and mitochondrial morphology. *J Biol Chem*. 2007;282:21583-21587.
32. Melck D, Rueda D, Galve-Roperh I, De Petrocellis L, Guzman M, Di Marzo V. Involvement of the cAMP/protein kinase A pathway and of mitogen-activated protein kinase in the anti-proliferative effects of anandamide in human breast cancer cells. *FEBS Lett*. 1999;463:235-240.
33. Mackie K. Cannabinoid receptors: where they are and what they do. *Neuroendocrinology*. 2008;20(suppl 1):10-14.
34. Kashatus JA, Nascimento A, Myers LJ, et al. Erk2 phosphorylation of Drp1 promotes mitochondrial fission and MAPK-driven tumor growth. *Mol Cell*. 2015;57:537-551.
35. Prieto J, Leon M, Ponsoda X, et al. Early ERK1/2 activation promotes DRP1-dependent mitochondrial fission necessary for cell reprogramming. *Nat Commun*. 2016;7:11124.
36. Szeto HH, Liu S, Soong Y, Alam N, Prusky GT, Seshan SV. Protection of mitochondria prevents high-fat diet-induced glomerulopathy and proximal tubular injury. *Kidney Int*. 2016;90:997-1011.
37. Panov A, Schonfeld P, Dikalov S, Hemendinger R, Bonkovsky HL, Brooks BR. The neuromediator glutamate, through specific substrate interactions, enhances mitochondrial ATP production and reactive oxygen species generation in nonsynaptic brain mitochondria. *J Biol Chem*. 2009;284:14448-14456.
38. Wang CH, Wu SB, Wu YT, Wei YH. Oxidative stress response elicited by mitochondrial dysfunction: implication in the pathophysiology of aging. *Exp Biol Med*. 2013;238:450-460.
39. Koch M. Cannabinoid receptor signaling in central regulation of feeding behavior: a mini-review. *Front Neurosci*. 2017;11:293.
40. Cota D, Marsicano G, Tschop M, et al. The endogenous cannabinoid system affects energy balance via central orexigenic drive and peripheral lipogenesis. *J Clin Invest*. 2003;112:423-431.
41. Osei-Hyiaman D, Liu J, Zhou L, et al. Hepatic CB1 receptor is required for development of diet-induced steatosis, dyslipidemia, and insulin and leptin resistance in mice. *J Clin Invest*. 2008;118:3160-3169.
42. Jourdan T, Djaouti L, Demizieux L, Gresti J, Verges B, Degrace P. CB1 antagonism exerts specific molecular effects on visceral and subcutaneous fat and reverses liver steatosis in diet-induced obese mice. *Diabetes*. 2010;59:926-934.
43. Tam J, Vemuri VK, Liu J, et al. Peripheral CB1 cannabinoid receptor blockade improves cardiometabolic risk in mouse models of obesity. *J Clin Invest*. 2010;120:2953-2966.
44. Liu J, Zhou L, Xiong K, et al. Hepatic cannabinoid receptor-1 mediates diet-induced insulin resistance via inhibition of insulin signaling and clearance in mice. *Gastroenterology*. 2012;142:1218-1228.
45. Tam J, Cinar R, Liu J, et al. Peripheral cannabinoid-1 receptor inverse agonism reduces obesity by reversing leptin resistance. *Cell Metab*. 2012;16:167-179.
46. Janiak P, Poirier B, Bidouard JP, et al. Blockade of cannabinoid CB1 receptors improves renal function, metabolic profile, and increased survival of obese Zucker rats. *Kidney Int*. 2007;72:1345-1357.
47. Galloway CA, Yoon Y. Perspectives on: SGP symposium on mitochondrial physiology and medicine: what comes first, misshape or dysfunction? The view from metabolic excess. *J Gen Physiol*. 2012;139:455-463.
48. Yu T, Robotham JL, Yoon Y. Increased production of reactive oxygen species in hyperglycemic conditions requires dynamic change of mitochondrial morphology. *Proc Natl Acad Sci U S A*. 2006;103:2653-2658.
49. Yu T, Sheu SS, Robotham JL, Yoon Y. Mitochondrial fission mediates high glucose-induced cell death through elevated production of reactive oxygen species. *Cardiovasc Res*. 2008;79:341-351.
50. Molina AJ, Wikstrom JD, Stiles L, et al. Mitochondrial networking protects beta-cells from nutrient-induced apoptosis. *Diabetes*. 2009;58:2303-2315.
51. Decleves AE, Zolkipli Z, Satriano J, et al. Regulation of lipid accumulation by AMP-activated kinase [corrected] in high fat diet-induced kidney injury. *Kidney Int*. 2014;85:611-623.
52. Mount P, Davies M, Choy SW, Cook N, Power D. Obesity-related chronic kidney disease-the role of lipid metabolism. *Metabolites*. 2015;5:720-732.
53. Pagliarini DJ, Calvo SE, Chang B, et al. A mitochondrial protein compendium elucidates complex I disease biology. *Cell*. 2008;134:112-123.
54. Forbes JM. Mitochondria-power players in kidney function? *Trends Endocrinol Metab*. 2016;27:441-442.
55. Hackenbrock CR. Ultrastructural bases for metabolically linked mechanical activity in mitochondria. I. Reversible ultrastructural changes with change in metabolic steady state in isolated liver mitochondria. *J Cell Biol*. 1966;30:269-297.
56. Parone PA, Da Cruz S, Tondera D, et al. Preventing mitochondrial fission impairs mitochondrial function and leads to loss of mitochondrial DNA. *PLoS One*. 2008;3:e3257.
57. Koopman WJ, Visch HJ, Verkaart S, van den Heuvel LW, Smeitink JA, Willems PH. Mitochondrial network complexity and pathological decrease in complex I activity are tightly correlated in isolated human complex I deficiency. *Am J Physiol Cell Physiol*. 2005;289:C881-C890.
58. Athanasiou A, Clarke AB, Turner AE, et al. Cannabinoid receptor agonists are mitochondrial inhibitors: a unified hypothesis of how cannabinoids modulate mitochondrial function and induce cell death. *Biochem Biophys Res Commun*. 2007;364:131-137.
59. Zaccagnino P, Corcelli A, Baronio M, Lorusso M. Anandamide inhibits oxidative phosphorylation in isolated liver mitochondria. *FEBS Lett*. 2011;585:429-434.
60. Tedesco L, Valerio A, Cervino C, et al. Cannabinoid type 1 receptor blockade promotes mitochondrial biogenesis through endothelial nitric oxide synthase expression in white adipocytes. *Diabetes*. 2008;57:2028-2036.
61. Lipina C, Hundal HS. Modulation of cellular redox homeostasis by the endocannabinoid system. *Open Biol*. 2016;6:150276.
62. Carracedo A, Geelen MJ, Diez M, Hanada K, Guzman M, Velasco G. Ceramide sensitizes astrocytes to oxidative stress: protective role of cannabinoids. *Biochem J*. 2004;380:435-440.
63. Kim SH, Won SJ, Mao XO, Jin K, Greenberg DA. Involvement of protein kinase A in cannabinoid receptor-mediated protection from oxidative neuronal injury. *J Pharmacol Exp Ther*. 2005;313:88-94.
64. Mukhopadhyay P, Pan H, Rajesh M, et al. CB1 cannabinoid receptors promote oxidative/nitrosative stress, inflammation and cell death in a murine nephropathy model. *Br J Pharmacol*. 2010;160:657-668.
65. Di Marzo V, De Petrocellis L, Fezza F, Ligresti A, Bisogno T. Anandamide receptors. *Prostaglandins Leukot Essent Fatty Acids*. 2002;66:377-391.
66. Han XJ, Lu YF, Li SA, et al. CaM kinase I alpha-induced phosphorylation of Drp1 regulates mitochondrial morphology. *J Cell Biol*. 2008;182:573-585.
67. Wang W, Wang Y, Long J, et al. Mitochondrial fission triggered by hyperglycemia is mediated by ROCK1 activation in podocytes and endothelial cells. *Cell Metab*. 2012;15:186-200.
68. Frieden M, James D, Castelbou C, Danckaert A, Martinou JC, Demaurex N. Ca(2+) homeostasis during mitochondrial fragmentation and perinuclear clustering induced by hFis1. *J Biol Chem*. 2004;279:22704-22714.
69. Fisar Z, Singh N, Hroudova J. Cannabinoid-induced changes in respiration of brain mitochondria. *Toxicol Lett*. 2014;231:62-71.
70. Benard G, Massa F, Puente N, et al. Mitochondrial CB(1) receptors regulate neuronal energy metabolism. *Nat Neurosci*. 2012;15:558-564.
71. Koch M, Varela L, Kim JG, et al. Hypothalamic POMC neurons promote cannabinoid-induced feeding. *Nature*. 2015;519:45-50.

72. Mendizabal-Zubiaga J, Melser S, Benard G, et al. Cannabinoid CB1 receptors are localized in striated muscle mitochondria and regulate mitochondrial respiration. *Front Physiol*. 2016;7:476.

SUPPORTING INFORMATION

Additional supporting information may be found online in the Supporting Information section at the end of the article.

How to cite this article: Drori A, Permyakova A, Hadar R, Udi S, Nemirovski A, Tam J. Cannabinoid-1 receptor regulates mitochondrial dynamics and function in renal proximal tubular cells. *Diabetes Obes Metab*. 2019;21:146–159. https://doi.org/10.1111/dom.13497